J. Great Lakes Res. 33:722–735
Internat. Assoc. Great Lakes Res., 2007

Satellite SAR Remote Sensing of Great Lakes Ice Cover, Part 1. Ice Backscatter Signatures at C Band

Son V. Nghiem[1,*] and George A. Leshkevich[2]

[1]*Jet Propulsion Laboratory*
California Institute of Technology
4800 Oak Grove Drive, MS 300-235
Pasadena, California 91109

[2]*National Oceanic and Atmospheric Administration*
Great Lakes Environmental Research Laboratory
2205 Commonwealth Blvd.
Ann Arbor, Michigan 48105

ABSTRACT. *For remote sensing of Great Lakes ice cover, a field experiment campaign was conducted in the 1997 winter season across the Straits of Mackinac and Lake Superior. The campaign was coordinated in two expeditions on two different United States Coast Guard icebreaker vessels, the* Biscayne Bay *in February and the* Mackinaw *in March. Aboard these icebreakers, the Jet Propulsion Laboratory C-band polarimetric scatterometer was used to measure backscatter signatures of various ice types and open water at incidence angles from 0° to 60°. The radar measurements include incidence angles and polarizations of spaceborne Synthetic Aperture Radars (SAR) on ERS, RADARSAT, and Envisat satellites. The radar data together with* in situ *measurements form a signature library that can be used to interpret SAR data for ice classification and mapping. Results are presented for backscatter signatures of Great Lakes ice types from thin lake ice to thick brash ice with different snow-cover and surface conditions. The signature library indicates that several ice types can be identified with multi-polarization SAR data; however, single-polarization data can result in misclassification of ice and open water at different ranges of incidence angle and wind conditions. For incidence angles larger than 30°, thick brash ice, the most difficult for icebreaking operations and the most hazardous for ship navigation, can be uniquely identified by co-polarized backscatter for all wind conditions below the gale force.*

INDEX WORDS: *Great Lakes, ice, Synthetic Aperture Radar (SAR), ERS-2, RADARSAT, C-band polarimetric scatterometer, classification, remote sensing.*

INTRODUCTION

The Laurentian Great Lakes, with their vast natural resources, contribute significantly to the economic and recreational activities of North America. Ice cover in the Great Lakes is the most obvious seasonal transformation of the physical characteristics of the lakes. Ice cover has a major impact on lake-atmosphere interactions affecting regional climate (Shen *et al.* 1998), ecology (Crowder and Painter 1991, Vanderploeg *et al.* 1992), water level changes (Derecki and Quinn 1986), fisheries management (Brown *et al.* 1993), ice jams (Daly 1992), coastal erosion (Reimnitz *et al.* 1991), toxin distribution (Crane and Sonzogni 1992), as well as the hydropower industry (Assel *et al.* 1983), and shipping industry (Cooper *et al.* 1975).

The Great Lakes are the world's largest freshwater surface, covering an enormous area of 245,000 km^2. The large-scale nature of the ice cover problem in large lakes and in extensive waterways demands the use of satellite SAR data to satisfy both the required high resolution and the large areal coverage simultaneously. A satellite SAR can image the ice cover over the Great Lakes with a nominal resolution of 100 m or less (depending on data acquisition mode) and a swath width of up to 500 km. Because of its high resolution, SAR is appropriate

*Corresponding author. E-mail: son.v.nghiem@jpl.nasa.gov

to monitor ice navigation hazards in shipping lanes in lakes and rivers. Moreover, microwave SAR has the capability to penetrate clouds with negligible atmospheric effects. The all-weather, day-and-night sensing capability of SAR makes it well suited to the short daylight and cloud dominated winter conditions in the Great Lakes region.

Most of the early ice classification and mapping studies were done by subjective visual interpretation of satellite and other remotely sensed data. Starting in the mid-1970s, a series of studies, including field studies and computer digital image processing, explored techniques and algorithms to classify and map freshwater ice cover using LANDSAT and Advanced Very High Resolution Radiometer (AVHRR) optical data and later, ERS-1/2 and RADARSAT SAR data (Leshkevich and Nghiem (Part 2) 2007, and references therein). Past, present, and future spaceborne SARs aboard the ERS-1, ERS-2, RADARSAT-1, RADARSAT-2, and Envisat satellites can acquire radar images of the Great Lakes with different incidence angles, resolutions, and swath widths. All of these SARs operate at C band and measure backscatter with single or multiple polarizations. Therefore, it is imperative to obtain a library of C-band backscatter signatures for different ice types to interpret satellite SAR data for ice identification, classification, and mapping. With this objective, the Jet Propulsion Laboratory (JPL) and the National Oceanic and Atmospheric Administration (NOAA) Great Lakes Environmental Research Laboratory (GLERL) carried out a field experiment in February-March 1997 using United States Coast Guard (USCG) icebreakers in the Straits of Mackinac and Lake Superior.

In this paper (Part 1), the 1997 Great LAkes Winter Experiment (GLAWEX'97) is described, and the signature library of backscatter together with physical characteristics of different ice types are presented. Ice identification is discussed in context of backscatter of open water over different wind conditions. The companion paper (Leshkevich and Nghiem 2007) will present applications of the backscatter library for ice classification and mapping using calibrated ERS-2 and RADARSAT-1 SAR data; thus, we focus on the co-polarized backscatter signatures of different ice types here.

DESCRIPTION OF GLAWEX'97

GLAWEX'97 was coordinated into two expeditions on two different United States Coast Guard Cutter (USCGC) icebreaker vessels, the USCGC *Biscayne Bay* in February and the USCGC *Mackinaw* (an Arctic-class icebreaker) in March. This field campaign provides the first comprehensive C-band radar-signature dataset together with ice characteristics for applications to lake-ice remote sensing.

The JPL C-band polarimetric scatterometer (CPolScat) was mounted on board the *Biscayne Bay* and the *Mackinaw* to measure the backscatter from ice and water. This scatterometer (Nghiem *et al.* 1997) is an accurate, well calibrated, and stable radar. The operating frequency is in C band, which is the same frequency band of ERS, RADARSAT, and Envisat SARs. Furthermore, the scatterometer has full polarimetric capability including both magnitude and phase measurements. Thus, CPolScat results will be applicable to ERS-1 and 2 SARs with vertical polarization, to the RADARSAT-1 SAR with horizontal polarization, to the Envisat SAR with multiple polarizations, and to RADARSAT-2 SAR with the full polarimetric capability.

The JPL CPolScat arrived at GLERL in early February 1997. Pre-experiment system tests and calibrations were carried out at GLERL. Then, the scatterometer system was transported to the ship dock and integrated on the USCGC *Biscayne Bay* in February 1997 and then on the USCGC *Mackinaw* in March 1997. Further system tests and calibrations were performed on board each ship after the system integrations. On the *Biscayne Bay*, the JPL radar was mounted on the port side (left side looking from the stern to the bow) of the ship. The CpolScat was operated from the engineering control room inside the ship. A video camera was mounted on the frame of the antenna pointed in the same direction as the antenna look direction, so that the ice could be observed from inside the control room on a television monitor. The video images were recorded on 8-mm and VHS VCR tapes at the same time. On the *Mackinaw*, the CPolScat was also mounted on the port side, and the radar control system was set up in a small room close to the radar. Figure 1 shows the radar system set up on the *Biscayne Bay* and the *Mackinaw*.

Both the radio-frequency (RF) subsystem and the antenna of CPolScat were mounted on a gimbaled structure and protected from moisture and wetness by plastic sheets. Furthermore, the RF subsystem was maintained at a constant temperature of 25°C by an internal temperature control system (Nghiem *et al.* 1997). The gimbaled structure allowed the control of the antenna in both azimuth and elevation. To set the antenna pointing direction, the scat-

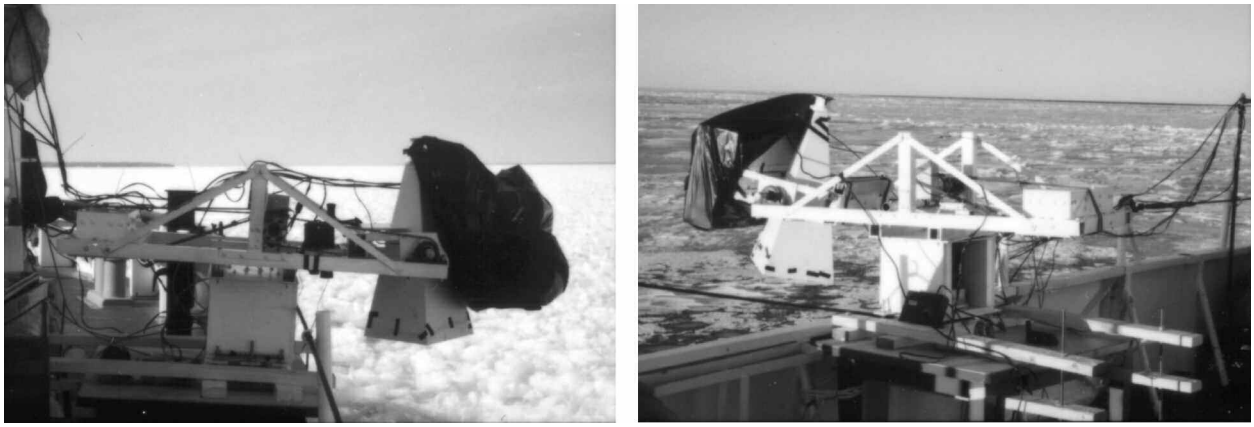

FIG. 1. JPL C-band polarimetric scatterometer mounted on the **Biscayne Bay** *shown on the left panel and the* **Mackinaw** *on the right panel.*

terometer operator adjusted the remote azimuth and incidence angle controllers until the desired direction was obtained. The incidence angle could be set with an accuracy of 0.02°. Using the video camera mounted with the antenna, the operator viewed the targeted areas on the television monitor. With this setup, the operator could ensure that cracks in the ice pack and artificially flooded surface made by ship motions would be excluded in backscatter measurements of the selected ice areas. These video observations of the ice conditions were augmented with written comments in the experiment log notes.

A Global Positioning System (GPS) receiver GARMIN GPS II unit was used to record the locations along the ship routes when the scatterometer data were taken. GPS data were downloaded to the same computer that controlled the radar in real time. The GPS data were plotted out on a map of the Great Lakes to determine locations of the ice types where radar data were collected. The com-

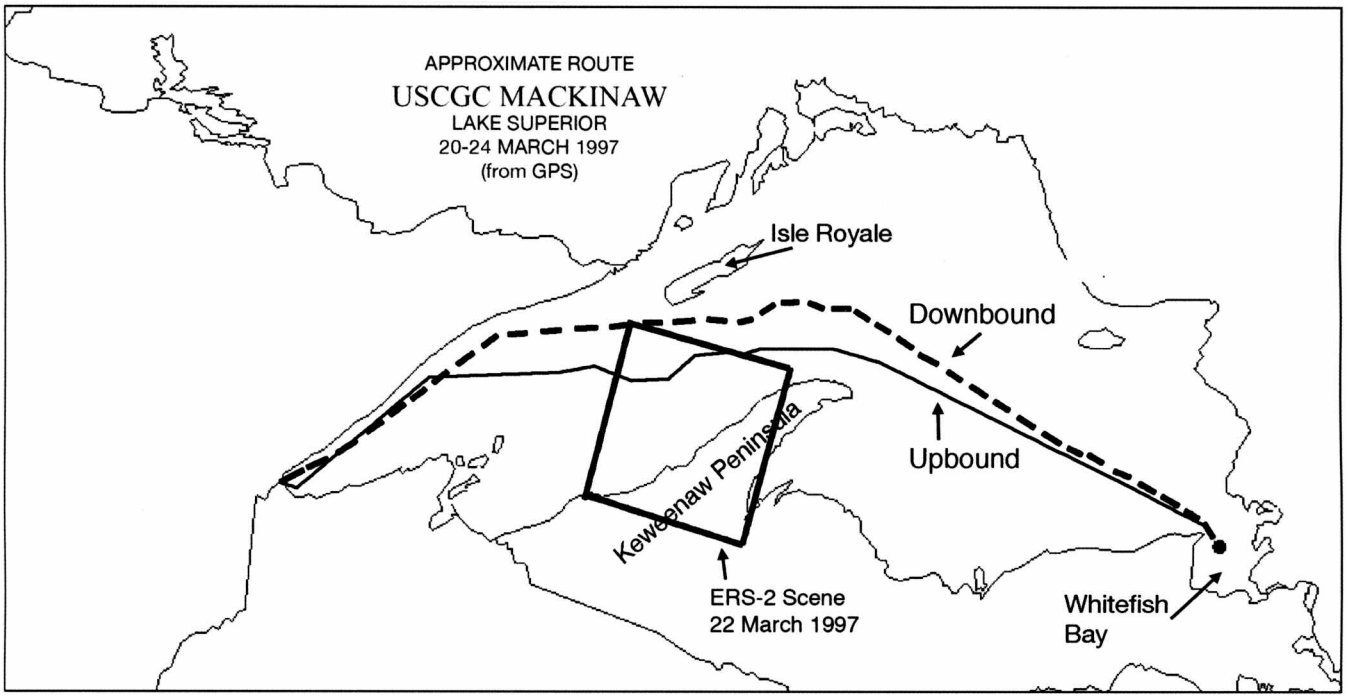

FIG. 2. Upbound (solid line) and downbound (dashed line) tracks of the USCGC Mackinaw together with ERS-2 SAR image area (box) over Lake Superior.

puter's internal clock was synchronized with the GPS time and both radar and GPS data were time tagged so that they can be correlated. An anemometer was used near the radar to measure *in situ* wind. The ship instruments also provided location, wind data, and temperature data. Figure 2 presents upbound and downbound tracks of the USCGC *Mackinaw* plotted on Lake Superior with the GPS data.

During the experiments, accurate calibration measurements were conducted to calibrate the scatterometer data. A trihedral corner reflector of known radar cross section was used for this purpose. The corner reflector was aligned exactly in the radar pointing direction with a laser pointer. Real time radar signals were displayed on a Hewlett-Packard network analyzer to verify the alignment by detecting the maximum radar returns. Furthermore, a metallic sphere was used as another calibration target to cross-validate the radar calibration. During the experiment on board the *Biscayne Bay,* the calibration measurements were taken while the ship docked at a port near De Tour Village in Michigan. The calibration targets were set up on the ground and the radar was on the port side of the ship. Background measurements were used in the coherent subtraction method to remove the background noise and significantly increase the signal-to-noise ratio of targeted areas (Nghiem *et al.* 1997). In the *Mackinaw* experiment, the calibration targets were setup on an open area at the back of the ship and microwave absorbers were used to avoid unwanted signals from reflections and multipath effects.

At each measurement location, surface truth data were obtained, and ice and snow thickness were measured. Photographs showing the layering structure of snow ice and lake ice with different amount of air inclusions were taken. The photograph in Figure 3 shows an example of the ice layering structure. Wind speed and temperature were recorded. We also took a number of snow thickness measurements over an area at a location during the *Biscayne Bay* experiment to determine the range of snow thickness distribution. Photographs were taken to estimate the surface roughness condition and snow coverage. For each set of radar measurements over an ice type, photographs were taken both in the near range coincident to the area of the radar footprint and in the far range showing the overall characteristics and condition of the ice type.

During GLAWEX'97, spaceborne SAR images were ordered and acquired in coordination with the field activities so that ice-mapping results from

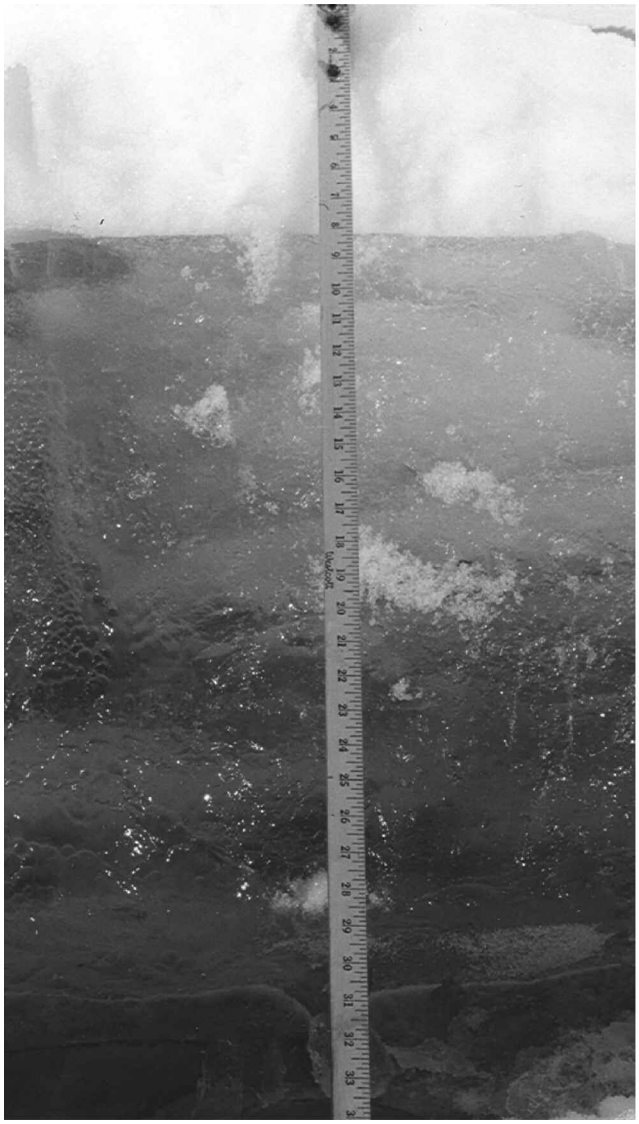

FIG. 3. Photograph of ice core showing ice layering structure.

SAR data can be validated with field measurements. For example, the box in Figure 2 shows the area of an ERS-2 SAR image overlapping the USCGC *Mackinaw* ship tracks. We will describe spaceborne SAR data collection in further detail in the companion paper (Leshkevich and Nghiem (Part 2) 2007). The total duration of this field campaign was approximately 1 month (2 weeks in February 1997 and 2 weeks in March 1997). The two experiments were jointly conducted and led by GLERL and JPL. The USCG organizations involved in this campaign were the USCGC *Mackinaw,* the USCGC *Biscayne Bay*, the USCG Traverse City Air Station for aerial survey, and the USCG

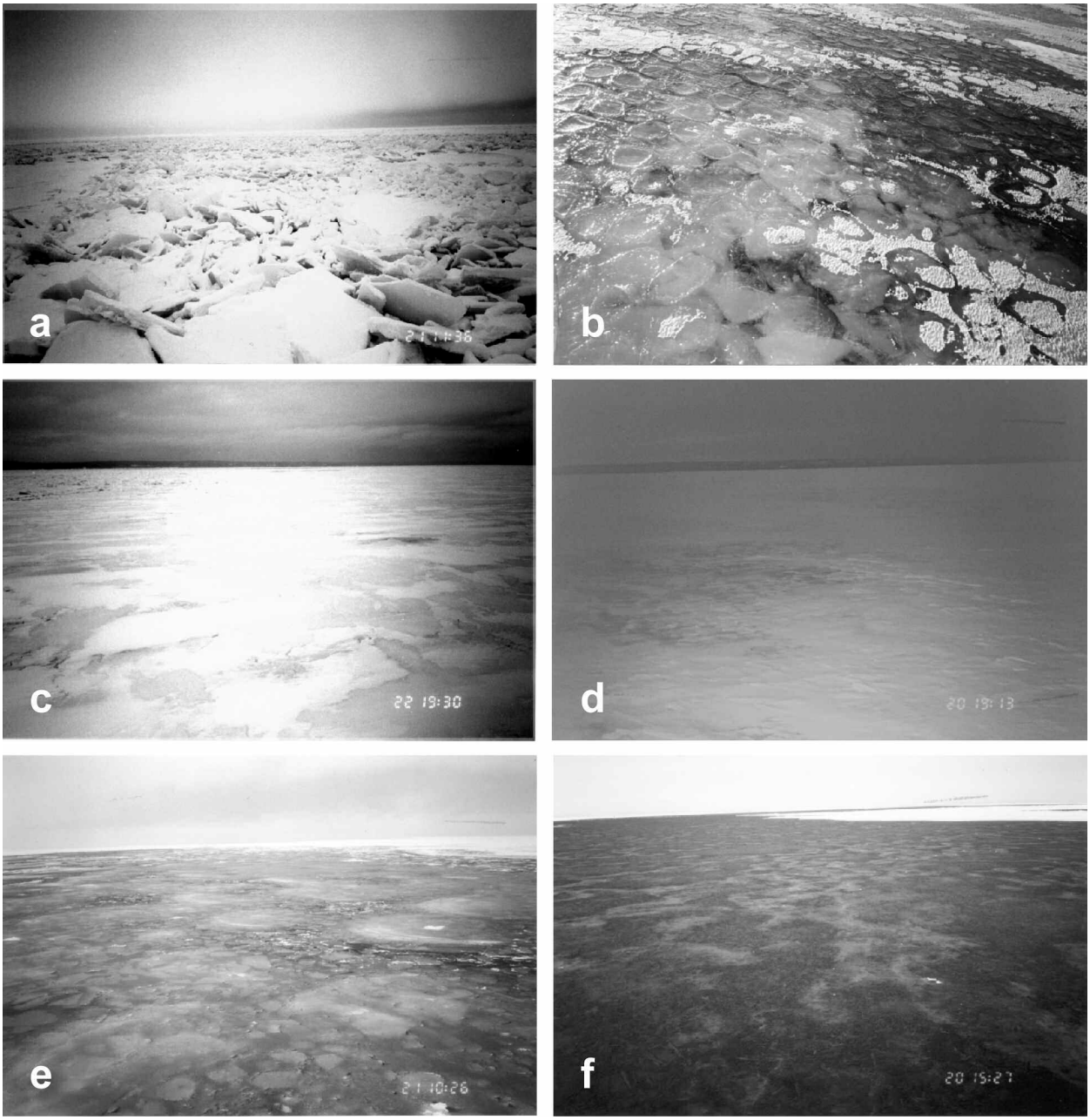

FIG. 4. Photographs of ice types measured during GLAWEX'97: (a) Brash ice, (b) pancake ice, (c) stratified ice, (d) lake ice with crusted snow, (e) consolidated ice floes, and (f) new lake ice.

Portage Ground Station in Michigan for ground support. As described above, GLAWEX'97 involved multiple coordinated components at lake, ground, air, and space levels.

ICE CHARACTERISTICS

Ice over the Great Lakes consists of mainly two basic kinds of ice: Lake ice that is mostly pure with very little air bubbles, and snow ice containing air inclusions from refrozen and densified snow. Depending on the ice formation processes, different ice types with different physical structures, layering or stratification, thickness, and surface conditions can have different backscatter signatures. We made backscatter measurements of different ice types with various snow cover, ice characteristics, and

TABLE 1. List of various ice types and calm water measured during GLAWEX'97.

Type	Thickness	Location	Surface Condition	Time
Brash ice	Up to > 5 m	47°37.9′N 87°48.3′W	Rubble field, crushed/broken ice plates, rough surface	3/21 11:32
Pancake ice	15–18 cm	47°50.9′N 87°53.1′W	Some snow areas, very rough edge at rim of pancake ice	3/23 18:32
Stratified ice	18–25 cm	46°56.1′N 91°39.4′W	Hard metamorphosed snow with mottled surface pattern, some relief	3/22 19:29
Lake ice with crusted snow	30–36 cm	46°28.4′N 84°34.4'W	Up to 5 cm snow cover, metamorphosed crusted surface	3/20 19:08
Consolidated ice floes	> 5 cm	47°36.7′N 87°40.0′W	Crescents of slush curd, mottled surface pattern, moist surface	3/21 10:25
New lake (black) ice	2.5 cm	46°43.0′N 84°51.0′W	Dark surface with some pattern of melted, refrozen snow—with relatively smooth surface	3/20 15:10
Calm water	0 cm, no ice	47°45.1′N 88°53.2′W	Calm surface, <1 $m \cdot s^{-1}$ wind speed at the time of radar measurement	3/23 13:10

surface roughness at 20 different locations. Ice and snow conditions at some locations were similar, and we present here results selected for different ice types commonly encountered over the Great Lakes. In all cases, extensive areas of each ice type were measured. Although the ice naming convention starts with documented definitions (U.S. Dept. Commerce 1971, U.S. Navy Hydrographic Office 1952, Canadian Ice Service 2004) deviation from standard terminology was made in some cases to better describe the ice type in terms of statigraphy, surface roughness, or other identifying characteristics as opposed to concentration. For example, a name like "patchy snow on snow ice over black ice" was used in an attempt to depict the ice type and layering or structure within the ice (along with a short name). Figure 4 shows the photographs of different ice types including: (a) brash ice, (b) pancake ice, (c) patchy snow on snow ice over black ice (stratified ice), (d) older lake ice with patchy and rough snow cover (lake ice with crusted snow), (e) rough consolidated ice floes (consolidated ice floes), and (f) black ice with some snow dusting on surface (new lake ice). Although some photographs were affected by sun glare, our purpose is to present the areas where radar measurements were made rather than taking pictures on the other side (no glare) of the ship where no data were collected. Table 1 lists the total thickness, location, surface condition, and time of measurement for each of the ice types. We describe their physical characteristics below:

(a) Brash ice: This ice type consisted of crushed and broken plates of lake ice and snow ice with 3–5 cm of snow. The size of the ice plates was about 1 to 2 m^2, and their thickness ranged from 15 to 30 cm. The ice field was heavily rafted and ridged by wind that deformed, compressed, and piled the ice plates to a thickness of several meters. Brash ice could be thicker than 5 m. Large fields of this ice type were encountered off the Keweenaw Peninsula.

(b) Pancake ice: The size of the pancake ranged from 30 to 60 cm. The pancake ice consisted of an 8-cm layer of snow ice frozen on 8–10 cm of lake ice. During the formation of pancake ice, the edge of the pancakes collided and rubbed against each other due to wind and wave actions making a raised and rough rim around each piece of pancake ice.

(c) Stratified ice: This ice type was horizontally stratified into level layers with 5–10 cm of snow ice layer on 12–15 cm of lake ice layer. The surface was covered by 1 cm

of hard metamorphosed snow with a mottled pattern and some relief. The top layer consisted of little pieces and chunks of ice frozen into the surface. We found large areas of this level ice type off Two Harbors, Minnesota. This ice type is quite common.

(d) Lake ice with crusted snow: This ice type consisted of 30-cm thick older lake ice with a thin patchy snow cover up to 5-cm thick. The surface snow layer was metamorphosed and crusted. Some areas of snow melted down to the ice surface. This ice type is common over the lakes.

(e) Consolidated ice flows: This ice type was an inhomogeneous mixture of broken snow ice floes frozen into a layer of lake ice. The size of the pieces of snow ice was quite variable, but it was about 30 cm on the average. Lake ice was 5-cm thick, and ice floes were thicker. The surface consisted of crescents of slush curd with a mottled surface pattern. At the time of measurement, the temperature was slightly above freezing, and there was some slush ice with ripples on the surface.

(f) New lake (black) ice: This was new lake ice that appeared black. There were some very thin patches of snow on the surface. The snow was melted then refrozen into a mottled surface probably from wind effects. Striations were observed on the surface with a dark tone that appeared like liquid water from a distance. At the time of measurement around 3:10 pm in the afternoon, the temperature was 6°C, and there was some slush from snowmelt.

For the cases of consolidated ice floes (e) and new lake ice (f), the moist surface might increase backscatter at small incidence angles (< 35°) and the effect would be small at larger incidence angles because the surface moist patches were thin, as compared to the backscatter when there was no surface moisture. Beside the above ice types, we also made measurements over a calm water surface (ice free). On the side of the ship where we acquired backscatter data, the water surface was protected by the ship, and the wind speed was low (0–1 $m \cdot s^{-1}$). There were more ripples on the water surface further out from the ship. On the windward side of the ship, the wind speed was 4 $m \cdot s^{-1}$. The air temperature was –4°C indicating that the water temperature at this location was warm, so that ice could not form on the water surface.

BACKSCATTER SIGNATURES

Scatterometer Data Processing

For each ice type, we obtained scatterometer data from 0° to 60° incidence angles. At each incidence angle, data were acquired in different azimuth directions scanned over the targeted area. For each antenna look direction, the data were coherently averaged by 20 times over 401 samples in the frequency domain over a bandwidth of 1 GHz. The measurements included both magnitudes and phases of the scattering matrix for all combinations in the linear polarization basis. We used the CPolScat polarimetric scatterometer data processor, which was modified for the particular data acquisition configuration and data format for the lake ice experiments, to process the raw frequency-domain data into gated time domain data to isolate the radar return from the targeted area.

The scatterometer data were calibrated both polarimetrically and radiometrically. Calibrated data consist of polarimetric backscattering coefficients including σ_{hh} and σ_{vv}, σ_{hv}, and magnitude and phase of σ_{hhvv}. Measured off-diagonal elements in the 2-by-2 scattering matrix were within 0.15 dB in magnitude and 3° in phase of each other, which practically satisfies the reciprocity principle. Ideally, the reciprocity requires a balance of 0.0 dB in magnitude and 0° in phase for these scattering elements. The channel balance between the horizontal and vertical polarizations was within ±0.2 dB. Backscatter results were obtained to construct a library of backscatter signatures with multi-polarizations and multi-incidence angles for the various ice types. Further details of CPolScat data processing were published in the literature (Nghiem *et al.* 1997).

Signatures of Great Lakes Ice

In view of applications to Great Lakes ice mapping with ERS and RADARSAT SAR data, we present results for co-polarized backscatter signatures of the ice types described in the Ice Characteristics section. We also show the ratio of co-polarized backscatter for potential applications to dual co-polarization data from Envisat SAR.

Figure 5 presents the backscatter signatures at the vertical polarization (σ_{vv} or VV) over a range of incidence angles from 20° to 60° for the ice types

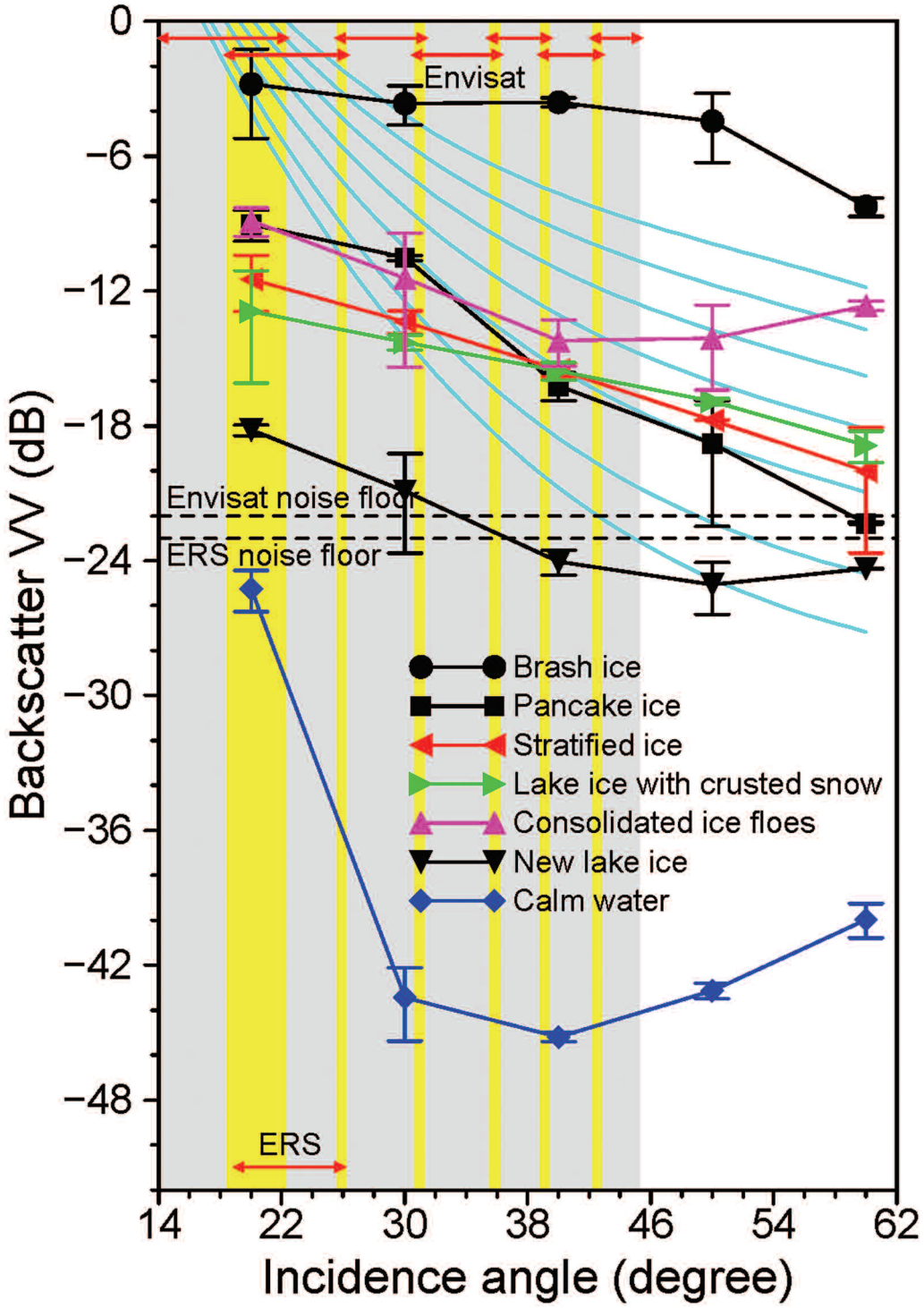

FIG. 5. Vertical-polarization backscatter signatures of Great Lakes ice and calm water. The ice types include brash ice, pancake ice, stratified ice, lake ice with crusted snow, consolidated ice floes, and new lake ice. The family of cyan curves represents CMOD3-H1 model values of vertical-polarization backscatter of ice-free water for neutral wind speeds of 2 m·s^{-1} and 4 m·s^{-1} to 24 m·s^{-1} in increments of 4 m·s^{-1} (lower to upper cyan curves). Red double arrows mark the ranges of incidence angles for ERS and Envisat SARs. The horizontal dashed lines delineate nominal σ_0-equivalent noise floors: –23 dB for ERS and –22 dB for Envisat. The background gray bands denote non-overlapping ranges of incidence angles of the seven swaths of Envisat SAR, and the yellow bands are for overlapping ranges of incidence angles between adjacent swaths.

shown in the photographs in Figure 4. Brash ice has the highest backscatter, well above the signatures of all other ice types. Backscatter of pancake ice is high at small incidence angles, but it decreases with a steep slope to a low value just above that of black ice at 60°. Backscatter of stratified ice, one of the most common ice types, varies from –11.5 to –20 dB over the whole range of incidence angles. Lake ice with crusted snow has a backscatter signature similar to that of stratified ice with slightly less change in backscatter as a function of incidence angle. Due to the roughness, C-band backscatter of consolidated ice floes can be relatively strong at the vertical polarization. New lake ice is virtually clear and contains almost no bubble or other volume scatterers in the ice layer, and thus it has the weakest backscatter among the different ice types. Over calm water (no wind to 1 $m \cdot s^{-1}$), the backscatter is the lowest of all because there was no ice cover, and the surface was very smooth. The increase in backscatter at large incidence angles (50-60°) was caused by the far range of the scatterometer measurements away from the ship where the wind was stronger.

Figure 6 shows the backscatter signatures at the horizontal polarization (σ_{hh} or HH) for the various ice types (Fig. 4). Backscatter of brash ice is also the highest for all ice types over the entire range of incidence angles. For pancake ice, backscatter has a steep slope at small incidence angles (< 40°), but it becomes a weak function of incidence angle at the large range (> 40°). In contrast, backscatter of stratified ice changes slightly over small incidence angles and has a larger decrease at large incidence angles. Backscatter of lake ice with crusted snow ice is similar to that of stratified ice at small (20°) and large (60°) incidence angles, while it is lower over the middle range of incidence angle (30–50°). Backscatter of consolidated ice floes varies from –11.1 dB at 20° to –18.7 dB at 60° and is primarily a linear function of incidence angle. New lake ice has the lowest backscatter among the different ice types. Furthermore, the slope of horizontal-polarization backscatter of black ice is the steepest. This backscatter characteristic of black ice is consistent with the surface scattering mechanism from the slightly rough interface at the ice-water or the air-ice layer boundary. Again, backscatter of calm water is the lowest of all as in the case of vertical-polarization backscatter.

When backscatter is contemporaneously measured at both vertical and horizontal polarizations over the same area, the co-polarized backscatter ratio r = VV/HH can be obtained. Figure 7 presents the backscatter ratio for each of the ice types. In the decibel (dB) domain, this ratio can be positive or negative because $r(dB)=10 \cdot \log(r) > 0$ when $r > 1$ and $r(dB) = 10 \cdot \log(r) < 0$ when $r < 1$. New lake ice, consolidated ice floes, or calm water has a large positive ratio at incidence angles larger than 30°, indicating the characteristic of surface scattering. For pancake ice, the behavior of the co-polarized ratio is complex due to complex structures in the surface and the volume of this ice type. The ratio of stratified ice is all negative over the range of incidence angles, indicating that the attenuation is low for this ice type and C-band electromagnetic waves can reach lower medium interfaces to enhance HH due to internal reflections. The backscatter ratio of lake ice with crusted snow is also negative or close to zero; however, the change of the ratio is opposite to that of stratified ice as a function of incidence angle.

APPLICATIONS TO SATELLITE SARS

A unique feature of this backscatter signature library of the different ice types is that the measurements cover a large range of incidence angles (up to 60°) with all polarizations in conjunction with *in situ* measurements and surface observations. The utility of this backscatter library is particularly important for applications to ice mapping using ERS data at the vertical polarization over a small range of incidence angles around 23° (red double arrow in Fig. 5) and RADARSAT data at the horizontal polarization over 20–49° (red double arrow in Fig. 6). The range of incidence angles in the backscatter library covers most of the Envisat SAR beams (Figs. 5–7) and also the future RADARSAT-2 SAR incidence angles including the extended-high modes up to 59.45° (Ali *et al.* 2004). Furthermore, the co-polarized backscatter ratio results will be useful to interpret data from both Envisat and RADARSAT-2 SARs, which have dual-polarization capabilities.

To investigate the capability to identify ice and open water, mean backscatter signatures (averaged over all azimuth directions) of ice-free water surface are included in Figures 5–7 for neutral wind speeds from 2 to 24 $m \cdot s^{-1}$ at 10-m height. Water backscatter is obtained from the empirical geophysical model function CMOD3-H1 (Long 1992) for the vertical polarization, and from a two-scale model (Plant 1986, Keller *et al.* 1992) modified by airborne SAR measurements (Nghiem and Bertoia 2001). These models are originally developed for

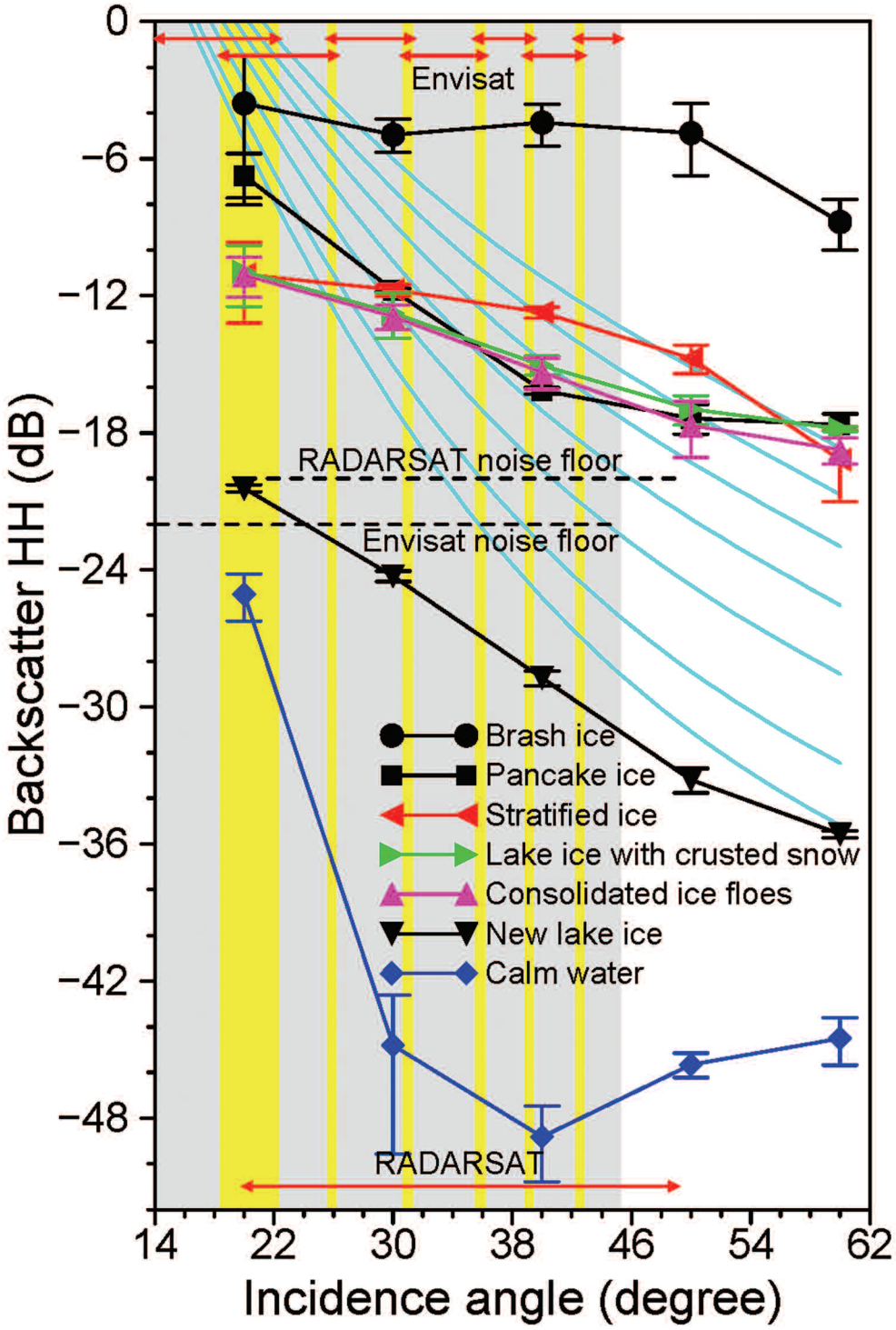

FIG. 6. Horizontal-polarization backscatter signatures of Great Lakes ice and calm water. The ice types include brash ice, pancake ice, stratified ice, lake ice with crusted snow, consolidated ice floes, and new lake ice. The family of cyan curves represents model values of horizontal-polarization backscatter of ice-free water for neutral wind speeds of 2 m·s^{-1} and 4 m·s^{-1} to 24 m·s^{-1} in increments of 4 m·s^{-1} (lower to upper cyan curves). Red double arrows mark the ranges of incidence angles for RADARSAT and Envisat SARs. The horizontal dashed lines delineate nominal σ_0-equivalent noise floors: –20 dB for RADARSAT and –22 dB for Envisat. The background gray bands denote non-overlapping ranges of incidence angles of the seven swaths of Envisat SAR, and the yellow bands are for overlapping ranges of incidence angles between adjacent swaths.

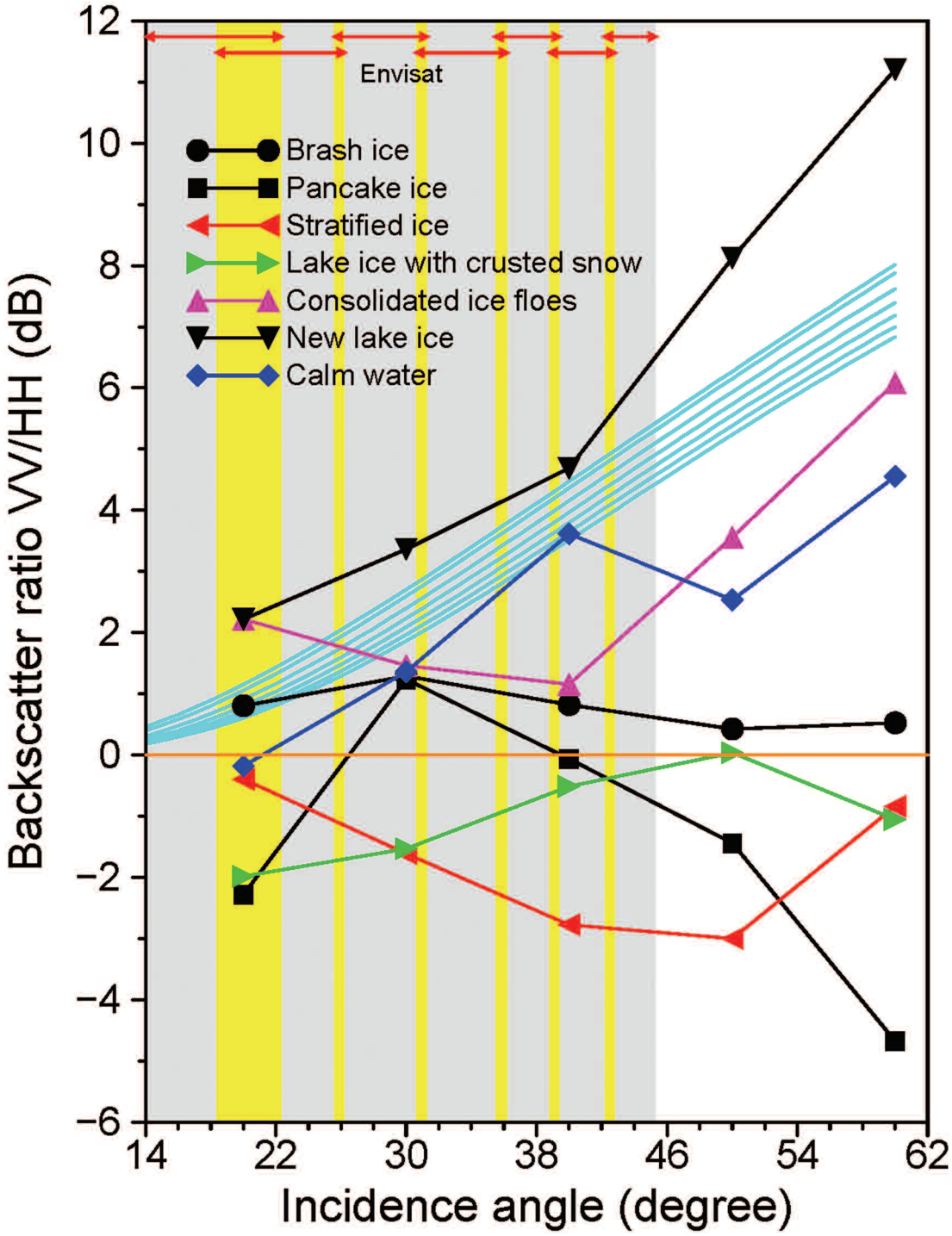

FIG. 7. Co-polarized backscatter ratios of Great Lakes ice and calm water. The ice types include brash ice, pancake ice, stratified ice, lake ice with crusted snow, consolidated ice floes, and new lake ice. The family of cyan curves represents model values of co-polarized backscatter ratios of ice-free water for neutral wind speeds of 2 $m \cdot s^{-1}$ and 4 $m \cdot s^{-1}$ to 24 $m \cdot s^{-1}$ in increments of 4 $m \cdot s^{-1}$ (upper to lower cyan curves). Red double arrows mark the ranges of incidence angles for Envisat SAR. The background gray bands denote non-overlapping ranges of incidence angles of the seven swaths of Envisat SAR and the yellow bands are for overlapping ranges of incidence angles between adjacent swaths.

saline water (seawater); however, salinity only affects backscatter weakly on a higher order (Donelan and Pierson 1987), and the error is small (Nghiem *et al.* 2004). These results are compared to ice backscatter signatures at different polarizations and incidence angles of the satellite SARs.

For ERS SAR operated at the vertical polarization, results in Figure 5 show that several ice types except brash ice can be identified from open water for wind speeds higher than 4 $m \cdot s^{-1}$. For backscatter higher than –4 dB, ERS vertical polarization data observe either brash ice or open water with higher wind speeds, but it cannot separate these two types and thus may cause a misclassification between brash ice and water. New lake ice (black ice) can be detected given the nominal σ_0-equivalent noise floor of –23 dB for ERS SAR (Meadows *et al.* 2004). New lake ice can also be separated from other ice types because of its low backscatter level. Below the ERS noise floor, backscatter of calm water cannot be measured by ERS and thus cannot be identified. These results indicated for backscatter around or lower than –18 dB, ERS can identify new lake ice or calm water in leads, which can be an easy route for icebreaker vessels to navigate through. Between –16 dB to –8 dB, several ice types can be observed in two groups: (1) stratified ice and lake ice with crusted snow with a thickness range of 18–36 cm in Table 1, and (2) consolidated ice floes and pancake ice with a thickness range of 5–18 cm. In view of Envisat SAR that has a wide swath and other SAR modes at the vertical polarization with incidence angles up to 45.3° (European Space Agency 2006), brash ice can be uniquely detected over beams 3–7 for wind speeds lower than gale force (17 $m \cdot s^{-1}$, Beaufort number 8) on the Beaufort Wind Scale. This capability is important since brash ice is the most difficult ice type for icebreaker vessels and its identification will facilitate the planning of ice breaking operations over the Great Lakes.

For RADARSAT SAR operated at the horizontal polarization, the plots in Figure 6 indicate that brash ice can be distinguished from open water for wind speed lower than the storm force (24 $m \cdot s^{-1}$, Beaufort number 10) over incidence angles larger than 30°. Thus, over this range of incidence angles, the horizontal polarization is better than the vertical polarization in identifying brash ice. Since wind speeds over storm force occur infrequently over the Great Lakes (Nghiem *et al.* 2004), RADARSAT SAR can detect brash ice most of the time at incidence angles larger than 30°. Backscatter values of both new lake ice and calm water are below the nominal noise floor of –20 dB for RADARSAT SAR. Below this value, RADARSAT SAR indicates that the lake surface is either new lake ice or calm water over the entire range of RADARSAT incidence angle. For incidence angles larger than 25°, RADARSAT SAR may misidentify different ice types with open water at different wind speeds; however, backscatter values of all ice types except new lake ice are above the noise floor. For Envisat SAR modes with the single horizontal polarization, the capability to identify different ice types and open water is similar to that of ERS SAR over the small range of incidence angle (Envisat SAR IS1 and IS2 beams). At larger incidence angles with the horizontal polarization, Envisat SAR and RADARSAT SAR are similar in terms of ice detection since there is only a small difference in the noise floors between these two SARs.

The current Envisat SAR and the future RADARSAT-2 SAR have the capability to acquire dual co-polarization data contemporaneously. Figure 7 shows results for the co-polarization backscatter ratio VV/HH. For Envisat SAR incidence angles larger than 30°, all of the ice types except new lake ice can be distinguished from open water with different wind speeds. Once ice is identified from open water, horizontal-polarization data can be used to identify stratified ice from lake ice with crusted snow, pancake ice, and rough thin ice. The stratified ice also has the lowest co-polarization ratio among the different ice types at incidence angles larger than 30° and less than 52°. These results indicate that Envisat or RADARSAT-2 dual co-polarization data are better for identifying and classifying different ice types. The backscatter signature library of the different ice types will be applied to satellite SAR data for ice mapping over the Great Lakes using satellite SAR data at C band (see Leshkevich and Nghiem (Part 2) 2007).

The results presented in this paper are mostly for ice conditions before ice decays in the candle stage due to significant melt. When the ice undergoes melting, wetness in the surface layer over ice cover may partially mask the C-band backscatter signatures of different ice types and thus decrease the capability of C-band SAR for ice identification and classification depending on the melting conditions. Radar data at C band or at a higher frequency such as Ku band (e.g., the QuikSCAT/SeaWinds scatterometer) are more sensitive to detect surface melt, and data at a lower frequency such as L band are less affected by surface wetness. In this regard, the

current L-band SAR such as the Advanced Land Observing Satellite (ALOS) Phased Array L-band Synthetic Aperture Radar (PALSAR) (Iragashi 2001) and the future L-band InSAR in the DESDynI Mission (National Research Council 2007) will be useful for Great Lakes ice classification and mapping.

ACKNOWLEDGMENTS

The authors gratefully acknowledge the U.S. Coast Guard Ninth District for providing the ground support, ship experimental platforms, and helicopter flights essential to the success of the experimental campaign. The research in this paper performed by Jet Propulsion Laboratory, California Institute of Technology, was sponsored by the National Oceanic and Atmospheric Administration (NOAA), through an agreement with the National Aeronautics and Space Administration. The research by the Great Lakes Environmental Research Laboratory was supported by NOAA. GLERL Contribution Number 1430.

REFERENCES

Ali, Z., Kroupnik, G., Matharu, G., Graham, J., Barnard, I., Fox, P., and Raimondo, G. 2004. RADARSAT-2 space segment design and its enhanced capabilities with respect to RADARSAT-1. *Can. J. Remote Sens. 30*(3):235–245.

Assel, R.A., Quinn, F.H., Leshkevich, G.A., and Bolsenga, S.J. 1983. *Great Lakes Ice Atlas.* NOAA, Great Lakes Environmental Research Laboratories, Ann Arbor, MI.

Brown, R.W., Taylor, W.W., and Assel, R.A. 1993. Factors affecting the recruitment of lake whitefish in two areas of northern Lake Michigan. *J. Great Lakes Res.* 19:418–428.

Canadian Ice Service. 2004. *Lake Ice Climatic Atlas, Great Lakes, 1973–2002,* Ottawa, Ontario, Canada.

Cooper, D.W., Mueller, R.A., and Schertler, R.J. 1975. Remote profiling of lake ice using an S-band short-pulser radar aboard an all terrain vehicle. *NASA Technical Memorandum* NASA TM X-71808.

Crane, J.L., and Sonzogni, W.C. 1992. Temporal distribution and fractionation of polychlorinated biphenyl congeners in a contaminated Wisconsin lake. *Chemosphere 24*(12):1921–1941.

Crowder, A., and Painter, D.S. 1991. Submerged macrophytes in Lake Ontario—Current knowledge, importance, threats to stability, and needed studies. *Can. J. Fish. Aquat. Sci. 48*(8):539–1545.

Daly, S.F. 1992. Observed ice passage from Lake Huron into the St-Clair river. *J. Great Lakes Res*. 18:61–69.

Derecki, J.A., and Quinn, F.H. 1986. Record St. Clair River ice jam of 1984. *J. Hydraulic Eng*. 112(12):1182–1194.

Donelan, M.A., and Pierson, W.J. 1987. Radar scattering and equilibrium ranges in wind-generated waves with application to scatterometry. *J. Geophys. Res*. 92(C5):4971–5029.

European Space Agency. 2006. *Envisat ASAR Product Handbook*, Issue 2.1. ESA Publication, 2006.

Iragashi, T. 2001. ALOS mission requirement and sensor specification. *Advances in Space Res*. 28(1):127–131.

Keller, M.R., Keller, W.C., and Plant, W.J. 1992. A wave tank study of the dependence of X band cross sections on wind speed and water temperature. *J. Geophys. Res. 97*(C4):5771–5792.

Leshkevich, G.A., and Nghiem, S.V. 2007. Satellite SAR remote sensing of Great Lakes ice cover, part 2. Ice classification and mapping. *J. Great Lakes Res.* 33:736–750.

Long, A.E. 1992. C-band V-polarized radar sea echo model from ERS-1 Haltenbalken Campaign. In *Proceedings, URSI Microwave Signature Conf.*, IGLS-Innsbruck, Austria.

Meadows, P.J., Rosich, B., and Santella, C. 2004. The ERS-2 SAR performance: The first 9 years. In *Proceedings, Envisat and ERS Symposium,* Salzburg, Austria.

National Research Council. 2007. *Earth Science and Applications from Space: National Imperatives for the Next Decade and Beyond.* The National Academies Press, Washington, D.C.

Nghiem, S.V., and Bertoia, C. 2001. Multi-polarization C-band SAR signatures of Arctic sea ice. *Can. J. Remote Sens., Focus Issue on Ice and Icebergs 2*(5):387–402.

———, Kwok, R., Yueh, S.H., Gow, A.J., Perovich, D.K., Kong, J.A., and Hsu, C.C. 1997. Evolution in Polarimetric Signatures of Thin Saline Ice under Constant Growth. *Radio Science* 32(1):127–151.

———, Leshkevich, G.A., and Stiles, B.W. 2004. Wind fields over the Great Lakes measured by the SeaWinds scatterometer on the QuikSCAT satellite. *J. Great Lakes Res.* 30:48–165.

Plant, W.J. 1986. A two-scale model of short wind-generated waves and scatterometry. *J. Geophys. Res.* 91:C9:10735–10749.

Reimnitz, E., Hayden, E., McCormick, M., and Barnes, P.W. 1991. Preliminary observations on coastal sediment loss through ice rafting in Lake Michigan. *J. Coastal Res*. 7(3):653–664.

Shen, H., Nghiem, S.V., Leshkevich, G.A., and Manore, M. 1998. *A Summary of Current Remote Sensing and Modeling Capabilities of the Great Lakes Ice Conditions.* Occasional Paper Series, Great Lakes Research Consortium, Great Lakes Program, State University of New York at Buffalo.

U.S. Department of Commerce. 1971. *Ice Glossary.* National Oceanic and Atmospheric Administration,

National Ocean Survey, Lake Survey Center, Detroit, MI (HO 75-602).

U.S. Navy Hydrographic Office. 1952. *A Functional Glossary of Ice Terminology.* Washington, D.C. (H.O. PUB. NO. 609).

Vanderploeg, H.A., Bolsenga, S.J., Fahnenstiel, G.L., Liebig, J.R., and Gardner, W.S. 1992. Plankton ecology in an ice-covered bay of Lake Michigan: utilization of a winter phytoplanton bloom by reproducing copepods. *Hydrobiol*. 243–244:175–183.

Submitted: 16 February 2007
Accepted: 20 June 2007
Editorial handling: William L. Schertzer